

Hydrothermal and Calcination Regimes and Characteristics of Nanohydroxyapatite Synthesized from *Salmon* bones

Nguyen Tri, Tran N. D. Trang, Nguyen H. D. Trinh, Lai T. Tung, Nguyen T. T. Van, Nguyen P. Anh, Nguyen D. Tan, Nguyen T. H. No, Huynh K. P Ha*

Received: 14 January 2020 / Received in revised form: 17 June 2020, Accepted: 20 June 2020, Published online: 24 June 2020

© Biochemical Technology Society 2014-2020

© Sevas Educational Society 2008

Abstract

Salmon bones – byproducts in food industries, was regarded as waste and will be discarded without fully utilizing it. From the approach of waste to wealth in the chemical compositions, the by-product can be employed as a cheap bioresource to form nanohydroxyapatite. In this paper, the influence of hydrothermal and calcined conditions on the structure of nano-hydroxyapatite synthesized from the salmon fishbone by the hydrothermal method was investigated. Various techniques such as X-ray diffraction (XRD), Fourier-transform infrared (FTIR) spectroscopy, field emission scanning electron microscopy (FE-SEM), transmission electron microscopy (TEM), and X-ray fluorescence spectrometry (XRF) were used to characterize the samples. XRD studies revealed that hydrothermal and calcined conditions affected the crystallinity as well as the purity of the hydroxyapatite. The suitable conditions for the synthesis of nanohydroxyapatite were proposed such as the hydrothermal at 120 °C for 8 hrs and calcined at 800 °C for 2 hrs. At the conditions, the hydroxyapatite had a spherical shape with the nanoparticle size in a range of 30–60 nm, and reached a BET surface area of 13.8 m².g⁻¹, a pore volume of 0.018 cm³.g⁻¹, and a pore diameter of 24.8 Å. The molar ratio of Ca/P in the hydroxyapatite was 1.64, which is the ratio one would expect for hydroxyapatite.

Key words: hydrothermal, calcination, nanohydroxyapatite, *Salmon* bones

Introduction

Nanotechnology is now considered as a future domain for treatment and diagnosis of many ailments (Ayaz, 2018). Nanoscience and nanotechnology have been promising as a rapidly growing field with its application in science and technology. Nanotechnology contributes to investigating unique and relatively new phenomena and providing novel applications (Abdussalam-Mohammed, 2019; Yang et al., 2019). Bio nanoparticles were considered as new materials with several properties that attracted researchers to work on them in the last decade. Nanohydroxyapatite is a bio-ceramic material, which has an almost identical chemical composition to the mineral component of bone (Dudek and Adamczyk, 2013). Hydroxyapatite gains considerable attraction due to its excellent properties, allowing synthetic hydroxyapatite to be used widely in biomedical applications and clinical surgery (Bingol and Durucan, 2012). Osteoporosis is considered a complex health issue which has been referred to as the silent disease of the century (Khani Jeihooni et al., 2018a). Osteoporosis is described by low bone mass and density (BMD) with micro architectural deterioration of bone tissue which causes enhanced bone fragility (Ahmad Ansari & Aamir Bin Sabir, 2017). Osteoporosis does not occur suddenly; it progresses gradually without obvious, subjective symptoms (Khani Jeihooni et al., 2018b). Hydroxyapatite is not only an osteoconductive, biocompatible, non-inflammatory, non-toxic, and non-immunogenic agents, but also bioactive, i.e. it has gotten the ability to form a direct chemical bond with living tissues (Sobczak et al., 2009). Besides, they are also applied in other fields such as adsorption and chemistry thanks to its excellent properties (Zhao et al., 2014).

Currently, the exploitation of hydroxyapatite based on waste materials has sparked worldwide interest, because it is an environmentally friendly process which can not only reduce costs but also save raw materials. Hydroxyapatite has been synthesized from various raw materials. The source of hydroxyapatite is derived from materials with high calcium content such as bovine bone (Jaber and Kovács, 2019; Maidaniuc et al., 2018), fishbone (Pal et al., 2017; Goto and Sasaki, 2016), fish scales (Muhammad et al., 2016; Pon-On et al., 2016), cuttlefish bone (Lagopati and Agathopoulos, 2019). Bovine and pig origins are often associated with religious sentiments and disease transmission (Gómez-

Nguyen Tri, Nguyen P. Anh

Institute of Chemical Technology, Vietnam Academy of Science and Technology, 01 Mac Dinh Chi Street, District 1, Ho Chi Minh City, Vietnam.

Tran N. D. Trang, Nguyen H. D. Trinh, Lai T. Tung, Nguyen D. Tan, Huynh K. P Ha*

Vietnam National University Ho Chi Minh City, Linh Trung Ward, Thu Duc District, Ho Chi Minh City, Vietnam.
Ho Chi Minh City University of Technology (HCMUT), 268 Ly Thuong Kiet Street, District 10, Ho Chi Minh City, Vietnam.

Nguyen T. T. Van, Nguyen T. H. No

Institute of Chemical Technology, Vietnam Academy of Science and Technology, 01 Mac Dinh Chi Street, District 1, Ho Chi Minh City, Vietnam.
Graduate University of Science and Technology, Vietnam Academy of Science and Technology, 18 Hoang Quoc Viet Street, Cau Giay District, Hanoi, Vietnam.

*Email: hkpha @ hcmut.edu.vn

Guillén et al., 2011). Fishbone sources are presumably much safer and suggest a low risk of disease transmission due to the wide evolutionary gap between fish and humans (Hoyer et al., 2012). Additionally, fish byproducts are abundant, and an application for these byproducts suitable for the biomedical application would reduce the threats of biohazards to humans and environmental pollution.

Different synthetic routes such as precipitation (Yelten-Yilmaz and Yilmaz, 2018), sol-gel (Asri et al., 2016), hydrothermal (Bensalah et al., 2018; Sunil and Jagannatham, 2016), solid-state (Pramanik et al., 2007), and mechanomechanical methods (Toriyama et al., 1996) have been employed to synthesis hydroxyapatite. Among them, hydroxyapatite is normally synthesized by hydrothermal methods. The temperature and duration of the reaction for hydrothermal treatment is an important variable for the characteristics of the resulting products (Wang et al., 2006; Ma M, 2012). If the reaction temperature is not high or the duration is not long enough, hydroxyapatite could not be synthesized, and it can result in a low specific surface area. The formation rate of different crystals and the aspect ratio of hydroxyapatite crystals also get affected by the temperature and duration of the reaction (Ren et al., 2012). Besides, the calcination conditions also affect the chemical and structural changes of hydroxyapatite. The temperature in a range of 500–650 °C is accepted as the whereas required to completely remove the organic phase of bone, further heating to 800 °C may be necessary to eliminate possible pathogenic agents and obtain protein-free samples (Ryu et al., 2019). Some investigations have shown that heating above 800 °C causes the formation of new mineral phases, e.i CaO or CaHPO₄. However, much fewer studies have investigated the comprehensive effect of hydrothermal and calcined conditions on the morphological, purity, and crystallinity of hydroxyapatite.

In this study, nano-hydroxyapatite was synthesized from the salmon fishbone by the hydrothermal method through alkaline hydrolysis. The influences of hydrothermal and calcined conditions on the structure and purity of hydroxyapatite were investigated.

Experimental

Fishbones after being collected were pretreated to remove inorganic impurities. Using enzymatic hydrolysis of protein to separate the organic content containing mainly protein from the remaining meat after the pile and the internal organs of the fish. The bone is filtered and washed, dried at 80 °C for 24 hours to

obtain dried fish bones. Then, the dried bone was finely ground into a powder to ensure particle sizes be less than 0.25 mm.

1.00 grams of finely ground dried fish bones ($d < 0.25$ mm) were dispersed in 50 ml of distilled water and stirred at room temperature at a stirring speed of 300 rpm for 30 minutes. Then, the 1% H₃PO₄ solution continuously dropwise into the reaction mixture, and the 5% NH₄OH solution was used to maintain pH = 10 during the synthesis duration. The volume of the H₃PO₄ solution used so that the molar ratio of Ca/P in the reaction mixture is 1.8. After the dropwise process has ended, the mixture was kept stirring at 300 rpm within 2 hours before being transferred into a Teflon bottle (100 mL). A Teflon bottle was packed in a tightly sealed autoclave and hydrothermally treated at T_h (°C) for t_h (hrs).

After that, the resulting precipitate was separated by centrifuging at a speed of 5000 rpm for 30 minutes and washed thoroughly with distilled water for several times until pH became 7. The collected precipitate was dried at 80 °C for 24 hours, and finally calcined at T_c (°C) for t_c (hrs) in the air with the heating rate of 5 °C.min⁻¹ and the airflow rate of 6 L.h⁻¹ to obtain hydroxylapatite. Finally, the sample was ball milled to nanohydroxyapatite. The nanohydroxyapatite samples synthesized from salmon fishbone are symbolized as following SHA-H(T_h-t_h)-C(T_c-t_c).

The components of raw fishbone, as well as nanohydroxyapatite, were determined using X-ray fluorescence (XRF) measurement using an ARL ADVANT'X Instrument (Thermo Scientific). X-ray powder diffraction (XRD) patterns were collected on Bruker D2 Phaser diffractometer using CuK α radiation ($\lambda = 0.154$ nm) in $2\theta = 10$ – 60° . The surface area, pore-volume, and average pore size of the catalysts were measured by nitrogen adsorption-desorption isotherm at -196 °C on Nova Station B, Quanta chrome Nova Win Instrument. Samples were degassed in a nitrogen flow at 200 °C for 2 hours before analyzing. The morphology of catalysts was characterized by field emission scanning electron microscopy (FE-SEM) using a Hitachi S4800 instrument and transmission electron microscopy (TEM) using a JEOL JEM 1400 instrument. Samples were put into ethanol, sonicated for thirty minutes, and dropped onto copper grids to make FE-SEM and TEM images. The Fourier transform infrared spectroscopy (FTIR) was carried out on a Tensor 27-Bruker spectrophotometer operated in the range of 400–4,000 cm⁻¹.

Results and Discussion

Determination of the synthesis conditions

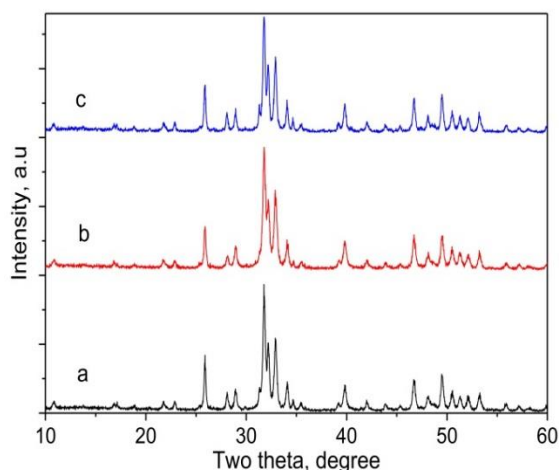


Figure 1. XRD patterns of nanohydroxyapatite samples synthesized by the hydrothermal at 120 °C for the different duration; a) SHA-H(120-7)-C(800-2), b) SHA-H(120-8)-C(800-2), c) SHA-H(120-9)-C(800-2).

The XRD patterns of nanohydroxyapatite samples synthesized by the hydrothermal at 120 °C for the different duration were shown in Figure 1. All samples had typical peaks of hydroxyapatite (JCPDS card No: 9–0432) with the strongest intensity at $2\theta = 31.4^\circ$. It was observed that the crystallinity of the samples was similar. The sample synthesized at 120 °C for 8 hrs (SHA-H(120-8)-C(800-2)) showed only hydroxyapatite peaks, while those of the samples synthesized at 120 °C for 7 hrs (SHA-H(120-7)-C(800-2)) and 9 hrs (SHA-H(120-9)-C(800-2)) showed the other peaks of monetite (CaHPO_4) (JCPDS card No: 70-0360). The XRD pattern of samples synthesized by the hydrothermal at different temperatures for 8h was shown in Figure 2. The sample synthesized at 120 °C did not contain any peaks other than those shown in the JCPDS reference file for hydroxyapatite. However, the XRD patterns of the samples treated at 100 and 140 °C show peaks attributed not only to hydroxyapatite but also to CaHPO_4 . The XRD peaks of all samples were well defined, indicating the

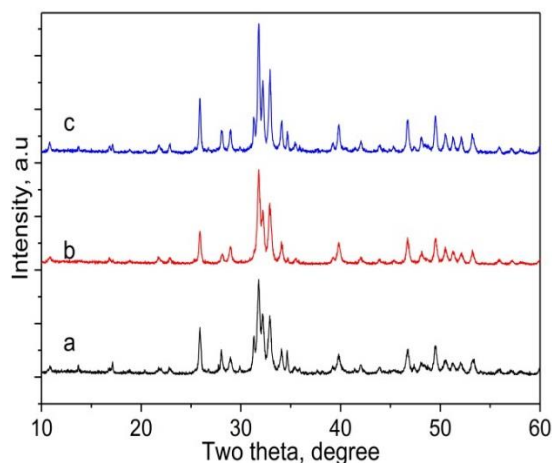


Figure 2. XRD patterns of nanohydroxyapatite samples synthesized by the hydrothermal at different temperatures for 8 hours; a) SHA-H(100-8)-C(800-2), b) SHA-H(120-8)-C(800-2), and c) SHA-H(140-8)-C(800-2).

samples were well crystallized. Therefore, considering the crystallinity and purity of the material, nanohydroxyapatite synthesized by the hydrothermal at 120 °C for 8 hrs was chosen for subsequent surveys. XRD pattern of the samples calcined at different temperatures for 2 hrs was shown in Figure 3. According to Figure 3, the calcining temperature plays an important role in the formation of hydroxyapatite. The crystallinity of SHA-H(120-8)-C(750-2) is lower than that of the samples calcined at 800 and 850 °C. The purity of SHA-H(120-8)-C(800-2) reached the highest, and it was almost no other crystal phase although the crystallinity of the material increased when the temperature increased to 850 °C (appear peaks of CaHPO_4). Similarly, the sample calcined for 2 hrs had the highest purity compared to the remaining samples. From obtained results, the suitable conditions for the synthesis of nanohydroxyapatite were proposed such as the hydrothermal at 120 °C for 8 hrs and calcined at 800 °C for 2 hrs.

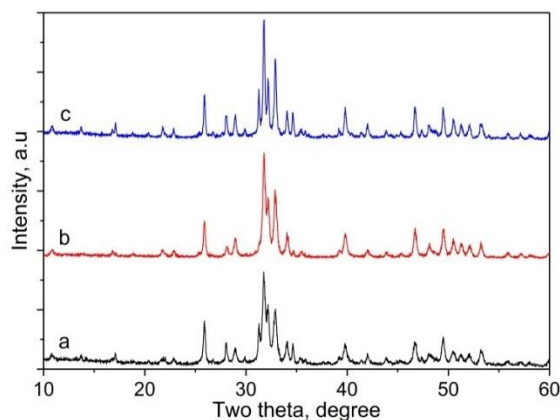


Figure 3. XRD patterns of nanohydroxyapatite calcined at different temperatures for 2 hours; a) SHA-H(120-8)-C(750-2), b) SHA-H(120-8)-C(800-2), and c) SHA-H(120-8)-C(850-2).

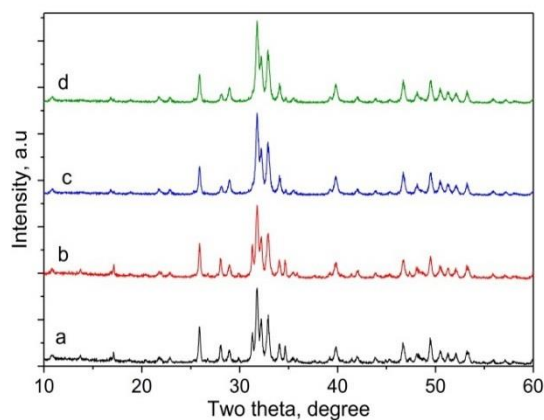


Figure 4. XRD patterns of nanohydroxyapatite samples calcined at 800 °C for different durations; a) SHA-H(120-8)-C(800-1), b) SHA-H(120-8)-C(800-1.5), c) SHA-H(120-8)-C(800-2), and d) SHA-H(120-8)-C(800-2.5).

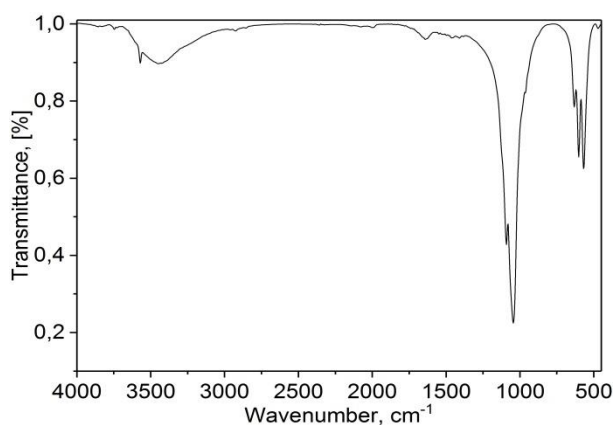
Characteristics of the nanohydroxyapatite sample synthesized at the suitable conditions

FT-IR spectra of the sample synthesized at the best conditions are presented in Figure 5a. FTIR utilized vibratory energy functional groups of constituent hydroxylapatite compounds, i.e. (PO_4^{3-}), (CO_3^{2-}), and (OH^-) groups. The spectra of the sample showed clear absorption peaks at 1095, 770, 605, and 560 cm^{-1} , which are generally assigned to the vibration of the PO_4^{3-} groups, are distinctly indicative of hydroxyapatite. On the other hand, the absorption band at 3443 and 3572 cm^{-1} corresponding to (OH^-) functional group. Besides, the absorption peak at 1653 cm^{-1} corresponding to (CO) functional group indicated a residual of carbonate (CO_3^{2-}). The results are consistent with the previous publication (Jamarun et al., 2016).

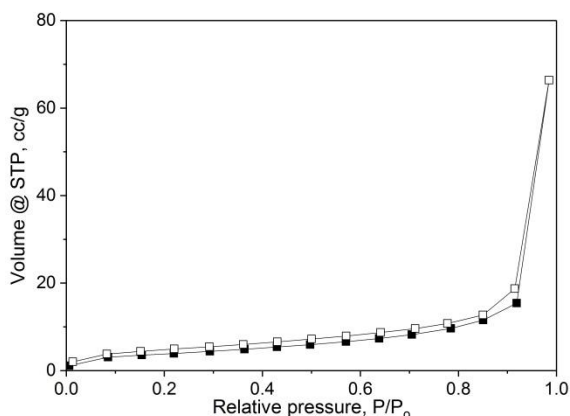
The N_2 adsorption-desorption isotherm of hydroxylapatite is shown in Figure 5b. The N_2 isotherm indicated a type II adsorption

profile, which is characteristic of macroporous materials or non-porous (Miyachi et al., 2019). The pore size distributions (PSD) of the specimens are plotted in Figure 5c. The pores were mostly distributed in the mesoporous range of 15–50 Å with the pore diameter of 24.8 Å. This pore size range was encouraging since the materials are advantageous for any application, especially in adsorption and catalysis. The sample had a BET surface area of 13.8 $\text{m}^2\cdot\text{g}^{-1}$ and a total pore volume of 0.018 $\text{cm}^3\cdot\text{g}^{-1}$.

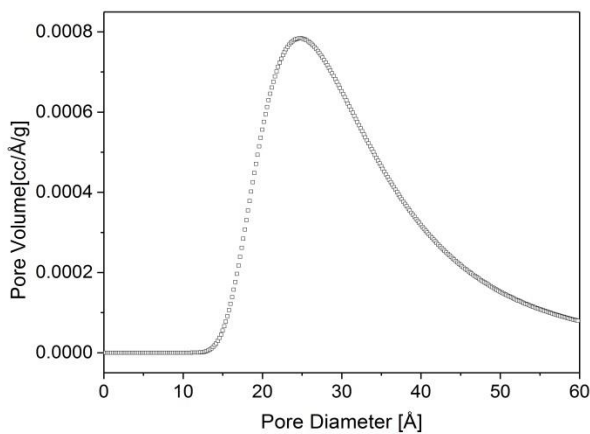
To study the morphology and size of the hydroxyapatite synthesized at the best conditions, the SEM and TEM images were shown in Figure 5d and 5e. The SEM image obtained from the hydroxyapatite showed the presence of nanosized particles with a uniform particle shape (Figure 5d) The particles were spherical shape and the size of the prepared nanoparticles was in a range of 30–60 nm. The TEM also confirmed the presence of the spherical shape morphology of the prepared hydroxyapatite with the particle size of around 40 to 60 nm (Figure 5e).



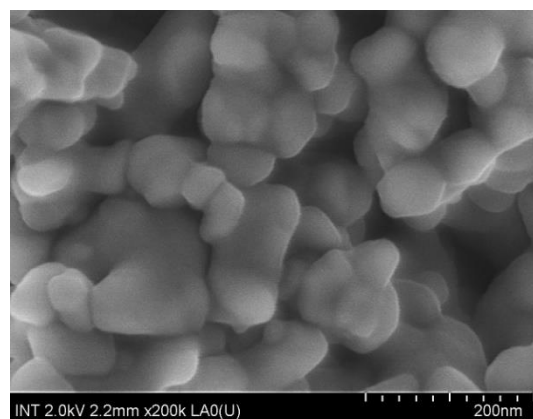
a)



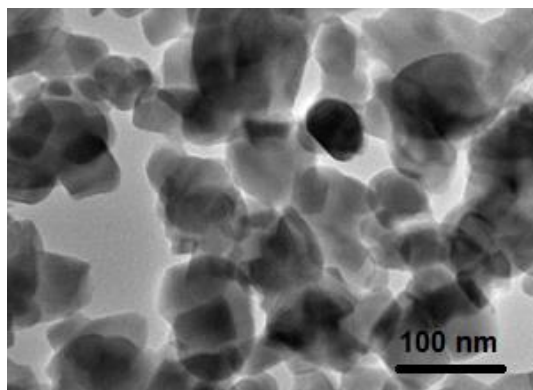
b)



c)



d)



e)

Figure 5. FTIR spectrum (a), N₂ adsorption/desorption isotherms (b), the BJH pore diameter distribution (c), FE-SEM image(d) and TEM image (e) of the nanohydroxyapatite sample synthesized at the suitable conditions

The chemical compositions of raw material and the hydroxyapatite synthesized at the best conditions are listed in Table 1. The raw material was mainly composed of Ca (72.4%), P (21.1%), and Mg (1.8%) components, which are needed to synthesize hydroxyapatite. After the synthesis process, the hydroxyapatite still maintained these components, and another component compared to the raw material, Na (2.2%). The observed molar ratio of Ca/P in hydroxyapatite reached 1.64, which is the ratio one would expect for hydroxyapatite. Besides, this ratio is similar to human bone (1.67), so it is suitable for addition to the human bone.

Table 1. The chemical composition of the raw material and the nano-hydroxyapatite synthesized at the suitable conditions.

Elements	Raw material, %	HA product, %
Ca	72.4	64.6
P	23.1	30.7
Mg	1.8	1.7
Sb	0.1	0
Cd	0.1	0
Sr	0.5	0.3
Si	0.6	0.5
S	0.6	0
Na	0.6	2.2
Zn	0.1	0
Sn	0.1	0
Sum	100	100

Conclusion

The biogenic hydroxyapatite was successfully synthesized from Salmon bones waste through a facile approach by the simple hydrothermal methods. It was revealed that the morphological,

purity, and crystallinity of the Salmon bone-derived hydroxyapatite is strongly correlated with the hydrothermal and calcined conditions. Based on the results obtained from various characteristics, the hydrothermal at 120 °C for 8 hrs and calcination at 800 °C for 2 hrs can be obtained hydroxyapatite with the highest crystallinity and purity. Finally, this paper proposed useful guidelines for the synthesis of Salmon bone-derived hydroxyapatite with propitious characteristics via the proper control of hydrothermal and calcined conditions to yield hydroxyapatite.

Acknowledgments

This research was supported by the Department of Science and Technology of Ho Chi Minh City under the contract number 78/2019/HĐ-QPTKHCN.

References

- Abdussalam-Mohammed W (2019) Review of Therapeutic Applications of Nanotechnology in Medicine Field and its Side Effects. *Journal of Chemical Reviews* 1: 243-251.
- Ahmad Ansari, A., & Aamir Bin Sabir, A. (2017). Scientific study of Unani formulations In the cases of osteoporosis. *Pharmacophore*, 8(2), 1-10.
- Asri, R. I. M., Harun, W. S. W., Hassan, M. A., Ghani, S. A. C., & Buyong, Z. (2016). A review of hydroxyapatite-based coating techniques: Sol-gel and electrochemical depositions on biocompatible metals. *Journal of the mechanical behavior of biomedical materials*, 57, 95-108.
- Ayaz, N. O. (2018). Beneficial impacts of n-3 polyunsaturated fatty acids on gold nanoparticles -induced liver injury by activating PPAR γ and Nrf2/HO-1 signaling pathways s. *Pharmacophore*, 9(1), 1-9.
- Bensalah, H., Bekheet, M. F., Younssi, S. A., Ouammou, M., & Gurlo, A. (2018). Hydrothermal synthesis of nanocrystalline hydroxyapatite from phosphogypsum waste. *Journal of environmental chemical engineering*, 6(1), 1347-1352.
- Bingol O R and Durucan C (2012) Hydrothermal synthesis of hydroxyapatite from calcium sulfate hemihydrate. *Am. J.*

- Biomed. Sci* 4: 50-59.
- Dudek A and Adamczyk L (2013) Properties of hydroxyapatite layers used for implant coatings. *Optica Applicata* 43:
- Gómez-Guillén, M. C., Giménez, B., López-Caballero, M. A., & Montero, M. P. (2011). Functional and bioactive properties of collagen and gelatin from alternative sources: A review. *Food hydrocolloids*, 25(8), 1813-1827.
- Goto T and Sasaki K (2016) Synthesis of morphologically controlled hydroxyapatite from fishbone by urea-assisted hydrothermal treatment and its Sr²⁺ sorption capacity. *Powder technology* 292: 314-322.
- Hoyer, B., Bernhardt, A., Heinemann, S., Stachel, I., Meyer, M., & Gelinsky, M. (2012). Biomimetically mineralized salmon collagen scaffolds for application in bone tissue engineering. *Biomacromolecules*, 13(4), 1059-1066.
- Jaber H L and Kovács T A (2019) Preparation and synthesis of hydroxyapatite bio-ceramic from bovine bone by thermal heat treatment. *Építőanyag* (Online) 98-101.
- Jamarun N, Azharman Z Et Al (2016) Effect of firing for synthesis of hydroxyapatite by precipitation method. *Oriental Journal of Chemistry* 32: 2095.
- Khani Jeihooni, A., Karimi, Sh., Kashfi, S. H., Mansourian, M., & Afzali Harsini, P. (2018a). Effectiveness of educational program based on Trans-Theoretical model in prevention of osteoporosis in women. *Journal of Advanced Pharmacy Education & Research*, 8(S2), 193-199.
- Khani Jeihooni, A., Khyali, Z., Kashfi, S. M., Forghani Fasaee, I., Moemenbellah-Fard, M. J., yazdi, N., & Afzali Harsini, P. (2018b). Quality of life in steoporotic patients compared with healthy people in an urban focus, South of Iran. *Journal of Advanced Pharmacy Education & Research*, 8(S2), 7-12.
- Lagopati N and Agathopoulos S (2019). Hydroxyapatite Scaffolds Produced from Cuttlefish Bone via Hydrothermal Transformation for Application in Tissue Engineering and Drug Delivery Systems. (Ed) Marine-Derived Biomaterials for Tissue Engineering Applications, Edn.: Springer
- Ma M-G (2012) Hierarchically nanostructured hydroxyapatite: hydrothermal synthesis, morphology control, growth mechanism, and biological activity. *International journal of nanomedicine* 7: 1781.
- Maidaniuc, A., Miculescu, F., Voicu, S. I., Andronescu, C., Miculescu, M., Matei, E., ... & Ciocan, L. T. (2018). Induced wettability and surface-volume correlation of composition for bovine bone derived hydroxyapatite particles. *Applied Surface Science*, 438, 158-166.
- Miyauchi, M., Watanabe, T., Hoshi, D., & Ohba, T. (2019). Irreversible adsorption of acidic, basic, and water gas molecules on calcium-deficient hydroxyapatite. *Dalton Transactions*, 48(47), 17507-17515.
- Muhammad, N., Gao, Y., Iqbal, F., Ahmad, P., Ge, R., Nishan, U., ... & Ullah, Z. (2016). Extraction of biocompatible hydroxyapatite from fish scales using novel approach of ionic liquid pretreatment. *Separation and Purification Technology*, 161, 129-135.
- Pal, A., Paul, S., Choudhury, A. R., Balla, V. K., Das, M., & Sinha, A. (2017). Synthesis of hydroxyapatite from Lates calcarifer fish bone for biomedical applications. *Materials Letters*, 203, 89-92.
- Pon-On, W., Suntornsaratoon, P., Charoenphandhu, N., Thongbunchoo, J., Krishnamra, N., & Tang, I. M. (2016). Hydroxyapatite from fish scale for potential use as bone scaffold or regenerative material. *Materials Science and Engineering: C*, 62, 183-189.
- Pramanik, S., Agarwal, A. K., Rai, K. N., & Garg, A. (2007). Development of high strength hydroxyapatite by solid-state-sintering process. *Ceramics International*, 33(3), 419-426.
- Ren, F., Ding, Y., Ge, X., Lu, X., Wang, K., & Leng, Y. (2012). Growth of one-dimensional single-crystalline hydroxyapatite nanorods. *Journal of Crystal Growth*, 349(1), 75-82.
- Ryu, G. U., Kim, G. M., Khalid, H. R., & Lee, H. K. (2019). The Effects of Temperature on the Hydrothermal Synthesis of Hydroxyapatite-Zeolite Using Blast Furnace Slag. *Materials*, 12(13), 2131.
- Sobczak, A., Kowalski, Z., & Wzorek, Z. (2009). Preparation of hydroxyapatite from animal bones. *Acta of Bioengineering and Biomechanics*, 11(4), 23-28.
- Sunil, B R., & Jagannatham, M. (2016) Producing hydroxyapatite from fish bones by heat treatment. *Materials Letters* 185: 411-414.
- Toriyama, M., Ravaglioli, A., Krajewski, A., Celotti, G., & Piancastelli, A. (1996). Synthesis of hydroxyapatite-based powders by mechano-chemical method and their sintering. *Journal of the European Ceramic society*, 16(4), 429-436.
- Wang Y, Zhang S, Wei K, Zhao N, Chen J, Wang X. Hydrothermal synthesis of hydroxyapatite nanopowders using cationic surfactant as a template. *Materials Letters*. 2006 Jun 1;60(12):1484-7.
- Yang, Y., Chawla, A., Zhang, J., Esa, A., Jang, H. L., & Khademhosseini, A. (2019). Applications of nanotechnology for regenerative medicine; healing tissues at the nanoscale. In *Principles of Regenerative Medicine* (pp. 485-504). Academic Press.
- Yelten-Yilmaz A., & Yilmaz S. (2018). Wet chemical precipitation synthesis of hydroxyapatite (HA) powders. *Ceramics International* 44: 9703-9710.
- Zhao, X. Y., Zhu, Y. J., Zhao, J., Lu, B. Q., Chen, F., Qi, C., & Wu, J. (2014). Hydroxyapatite nanosheet-assembled microspheres: Hemoglobin-templated synthesis and adsorption for heavy metal ions. *Journal of colloid and interface science*, 416, 11-18.